Platinum Single Atoms on Tin Oxide Ultrathin Film for Extremely Sensitive Gas Detection

Yongshan Xu,[a] Wei Zheng [a], Xianghong Liu* [a,b], Liqiang Zhang,[c] Lingli Zheng,[a] Chen Yang,[a] Nicola Pinna,[d] Jun Zhang* [a,b]

[a] College of Physics, Center for Marine Observation and Communications, Qingdao University, Qingdao 266071, China

[b] Key Laboratory of Advanced Energy Materials Chemistry (Ministry of Education), Nankai University, Tianjin 300071, China

[c] Clean Nano Energy Center, State Key Laboratory of Metastable Materials Science and Technology, Yanshan University, Qinhuangdao 066004, China

[d] Institut für Chemie and IRIS Adlershof, Humboldt-Universität zu Berlin, Brook-Taylor-Str. 2, 12489 Berlin, Germany

Corresponding author.
Email: xianghong.liu@qdu.edu.cn (X. Liu), jun@qdu.edu.cn (J. Zhang)

Experimental part

Materials: All chemical precursors were purchased from Nanjing Moyuan Scientific Instruments & Materials Co., Ltd. The SiO_2/Si wafers with resistivity of 1-20 Ω·cm were used for development of ALD deposited SnO_2 and Pt/SnO_2 thin films using tetrakis(dimethylamino)tin(IV) (TDMASn) (99%) and H_2O precursors, trimethyl(methylcyclopentadienyl)platinum(IV) ($MeCpPtMe_3$) (99%) and O_3 precursors.

ALD of SnO_2 films: The ALD process was carried out in a hot-wall, closed chamber type ALD reactor. Before the deposition, the SiO_2/Si wafers were cleaned in acetone, ethanol and distilled water for 10 minutes, respectively. TDMASn was used as precursor of Sn, H_2O was used as oxidant and high purity N_2 was used as the carrier and purge gas. The temperature of ALD chamber was kept at 150 ^oC, the container of TDMASn was heated to 45 ^oC and the gas lines were held at 150 ^oC. The SnO_2 thin films were deposited by alternating pulses of TDMASn and H_2O, with a 0.3 s pulse of TDMASn, and a 10 s exposure to fill the whole chamber, followed by a 0.5 s pulse of H_2O and a 10 s exposure. The cycles were separated by a 30 s purge of N_2. The thickness of SnO_2 thin films can be controlled by adjusting the number of ALD cycles. Therefore, 22, 50, 72 and 100 deposition cycles of SnO_2 were applied to SiO_2/Si wafers. The total deposition time for one cycle is 80.8 s and the growth rate is calculated to be ~0.18 nm for per cycle. Thus, the thickness of SnO_2 films in this study is 4, 9, 13 and 18 nm. After SnO_2 ALD deposition, the samples were processed by calcination at 500 ^oC for 30 minutes in air.

ALD of Pt on SnO_2 films: In a typical process, the as-prepared SnO_2 thin films were put into the reactor of the ALD instrument. The $MeCpPtMe_3$ was used as the precursor of Pt and O_3 was generated by an ozone generator using high purity O_2 gas and acted as the counter-reactant. The reactor was heated to 280 ^oC and the $MeCpPtMe_3$ was kept at 75 ^oC. Each ALD of Pt sequence was given by $MeCpPtMe_3$ pulse (1 s)-exposure (20 s)-N_2 purge (25 s)-O_3 pulse (1 s)-exposure (25 s)-N_2 purge (25 s). 5, 10 and 20 deposition cycles of Pt were applied to SnO_2 thin films. Finally, the prepared SnO_2/Pt films were reduced at 500 ^oC for 4 h under Ar/H_2 (10%) atmosphere and some samples were calcined in air under the same conditions for comparison.

Fabrication of electrodes: The SiO_2/Si wafers grown with SnO_2 and Pt/SnO_2 thin films was put into a Thermal Evaporation System to fabricate the electrodes using Ti/Au (10/30 nm). The whole thin film sensor preparation process was shown in **Figure S1**a-c.

Measurement and characterization: The morphologies were scanned by scanning electron microscope (SEM, Zeiss sigma 300). Transmission electron microscope (TEM) and high-resolution TEM (HRTEM) images were collected on a FEI JEM-2010. High-angle annular dark-field scanning TEM (HAADF-STEM) and energy dispersive X-ray spectroscopy (EDS) were performed on FEI TALOS F200. The X-ray photoelectron spectroscopy (XPS) was tested on a Thermo ESCALAB 250 with the $Al_{K\alpha}$ (1486.6 eV) anode. The surface morphology was observed by atomic force microscope (AFM, Nanosurf NaioAFM). Electron paramagnetic resonance (EPR) spectroscopy was collected on a Bruker A300.

Measurement of gas sensing performances: The gas sensing tests were carried out on a homemade instrument (**Figure S1**d). The sensor was connected to the test equipment (Keithley 2400) to measure the electrical current evolution. A ceramic heating plate (XH-RJ 101012) worked as a heater, which can tune the temperature by adjusting the heating voltage (Keithley 2231A). The test method adopts static test, and the concentration of the gas to be measured is generated by injecting a certain volume of liquid onto the heating plate. The gas sensing response (S) was defined as the ratio of the electrical resistance of the sensor in air (R_{air}) and in target gas (R_{gas}). The response-recovery time was defined as the time for the sensor to reach 90% of the final signal.

Calculation of the liquid volume

The volume of liquid (V) required for a given gas concentration (C) is calculated as follow:

$$V = \frac{PV_oCM}{RT\rho}$$

where P is the standard atmospheric pressure, V_o the volume of the test chamber, M the molar mass of target gases, R the gas constant, T the ambient temperature, and ρ the density of target gases.

Calculation of Debye length (L_D)

The Debye length L_D is a characteristic of a semiconductor material for a particular donor concentration and can be calculated as follow:[1]

$$L_D = \sqrt{\frac{\varepsilon_0 \varepsilon k_B T}{q^2 n_c}}$$

where k_B is Boltzmann's constant, ε the dielectric constant, ε_0 the permittivity of free space, T the operating temperature, q the electron charge, and n_c the carrier concentration, which corresponds to the donor concentration assuming full ionization.

The carrier concentration is obtained by Hall measurements.

Film thickness (nm)	Temperature (K)	Carrier concentration (m^{-3})	Mobility ($cm^2/V*s$)	Debye lenth (nm)
4	300	$2.17*10^{20}$	121.30	375.1
9	300	$9.22*10^{22}$	34.3	14.5

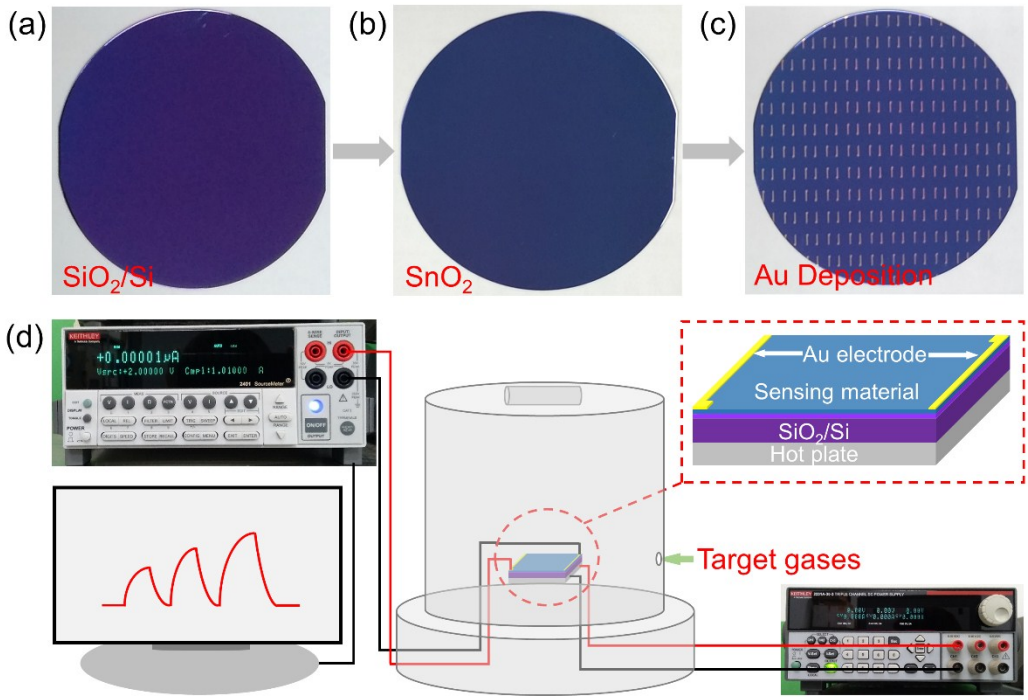

Figure S1. The images of (a) clean SiO_2/Si wafer and deposited with (b) SnO_2 thin film and (c) Au electrodes, (d) the schematic diagram of test device.

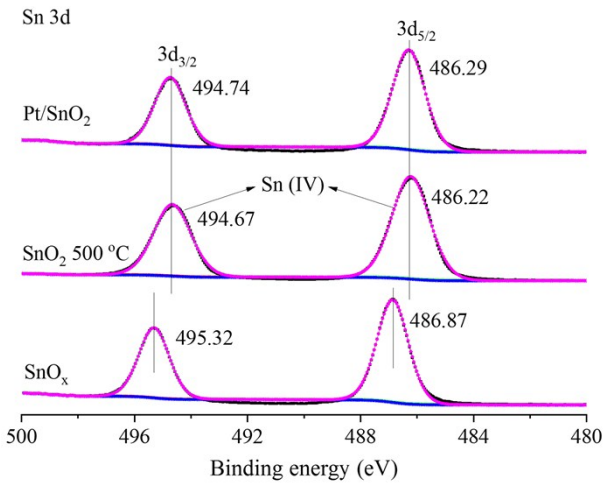

Figure S2. Core-level XPS spectra of Sn 3d of as-deposited SnO_X thin film by ALD, the SnO_2 thin film after annealing at 500 °C in air, and Pt/SnO_2 thin film.

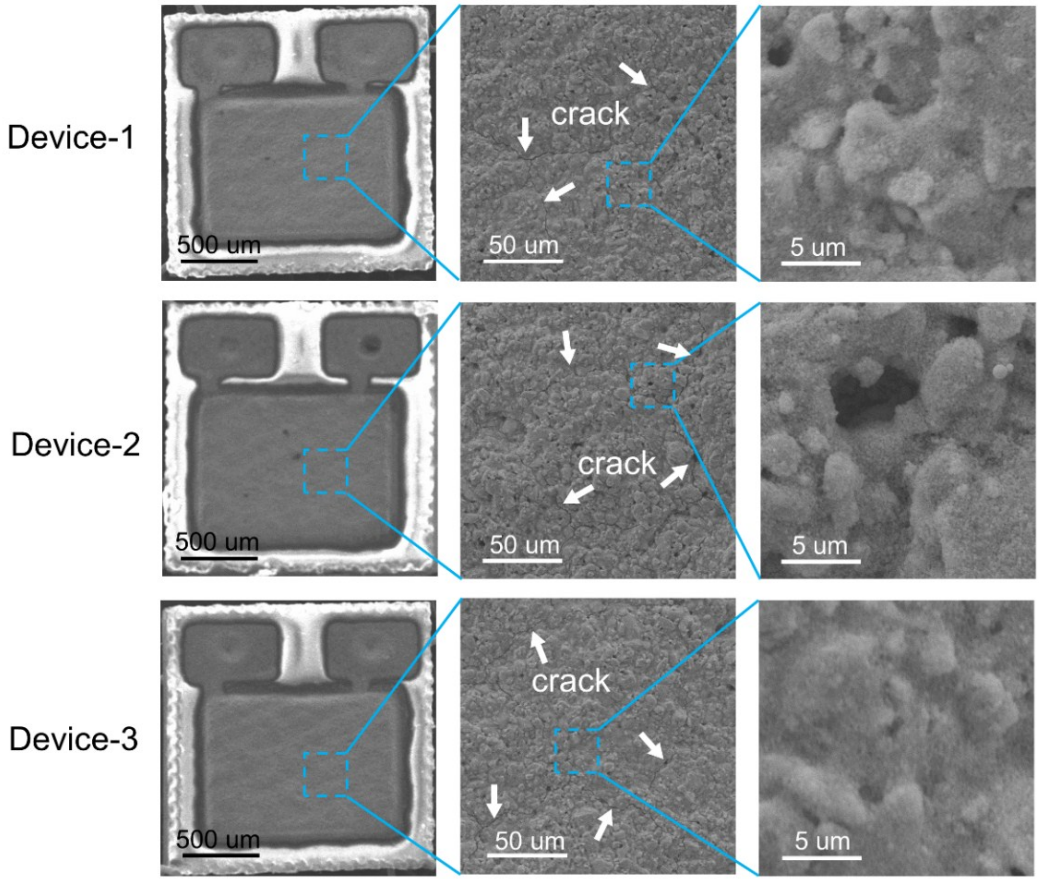

Figure S3. SEM of three commercial Figaro TGS 2602 sensors, showing the sensor element structure and the surface morphology of the sensing layers.

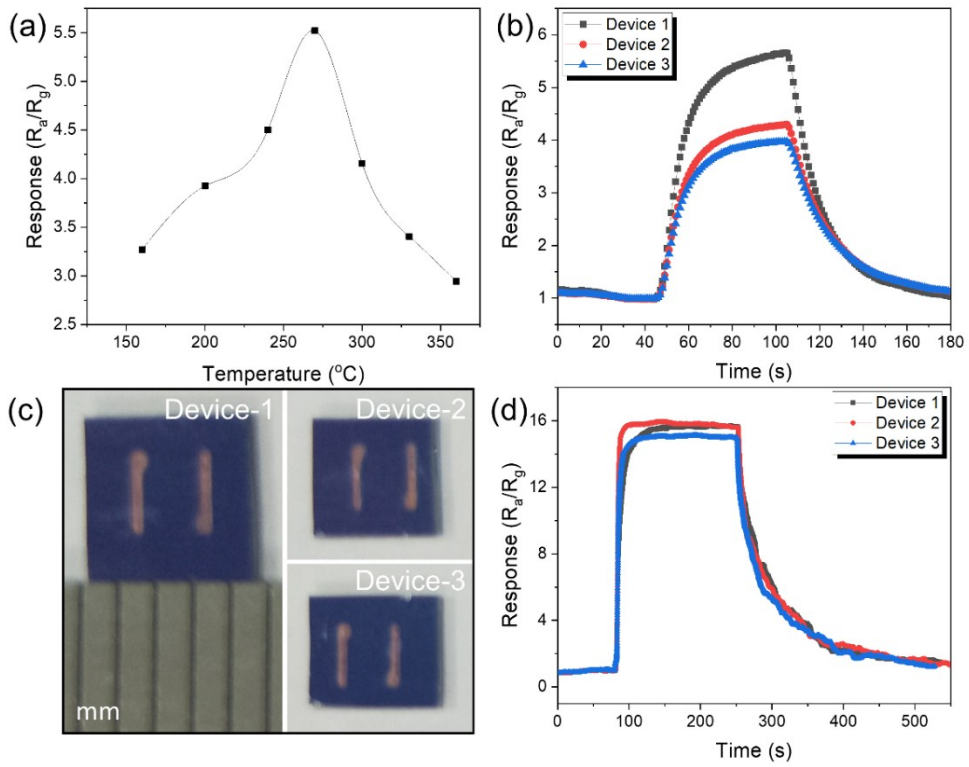

Figure S4. (a) Response of Figaro TGS 2602 sensor to 10 ppm TEA at different temperatures, (b) sensing transients to 10 ppm TEA TGS 2602 sensors, (c) the images of three SnO_2 thin film sensor and (d) corresponding sensing transients to 10 ppm TEA.

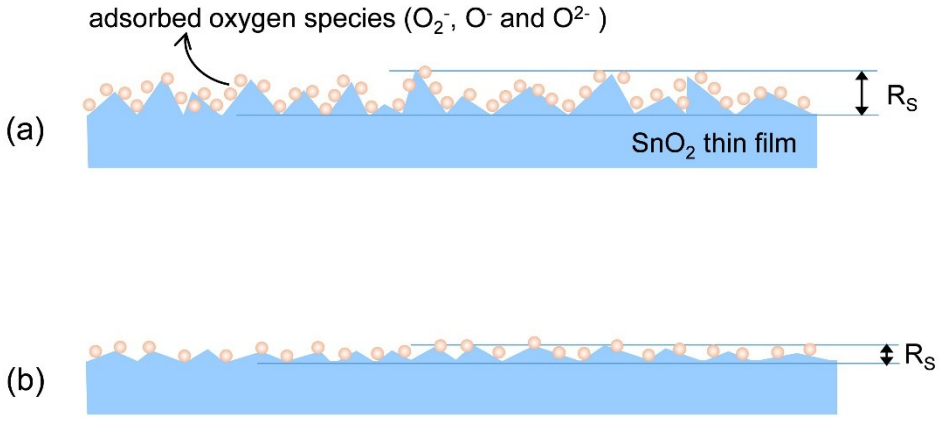

Figure S5. Schematic surface roughness of SnO_2 thin films with different amount of adsorbed oxygen species.

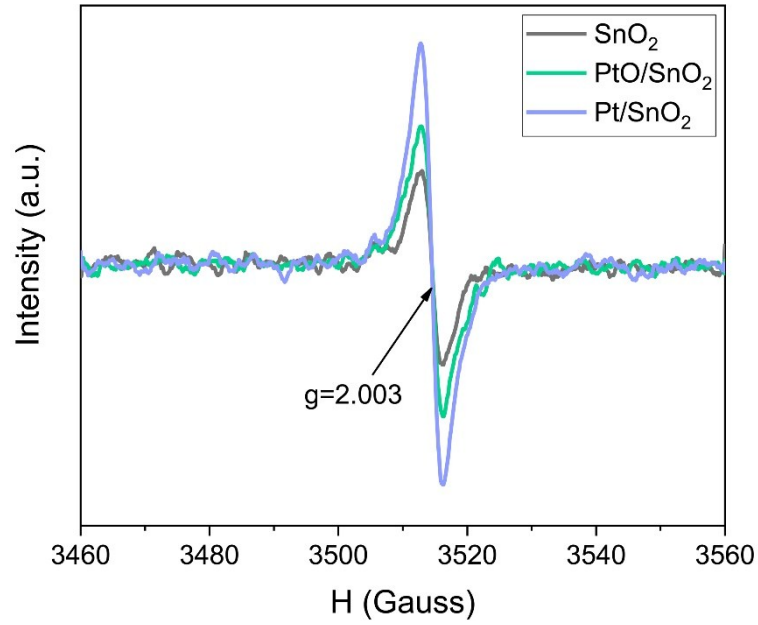

Figure S6. EPR spectra of Pt/SnO_2, PtO/SnO_2 and SnO_2 thin films.

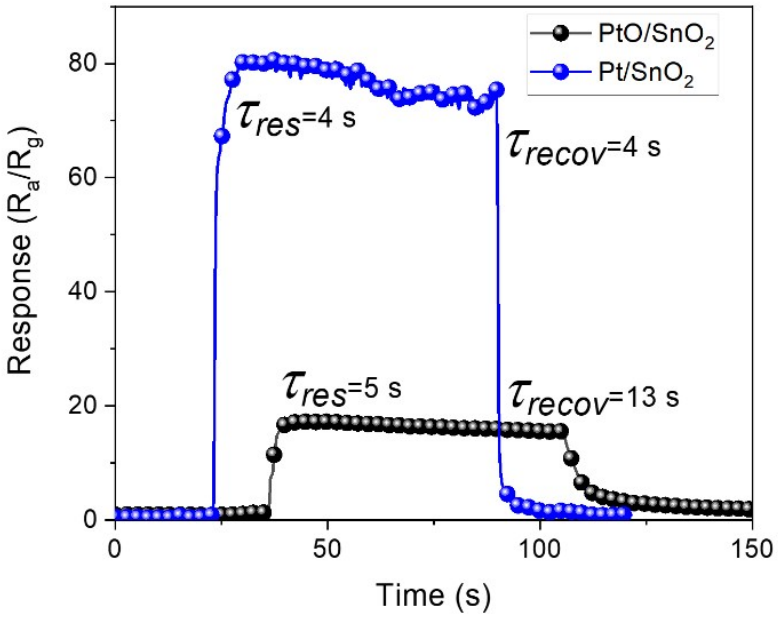

Figure S7. Dynamic transients on exposure to 5 ppm TEA of Pt/SnO_2 and PtO/SnO_2 thin films with 10 cycle of Pt ALD after annealing in Ar/H_2 and air at 500 ^{o}C.

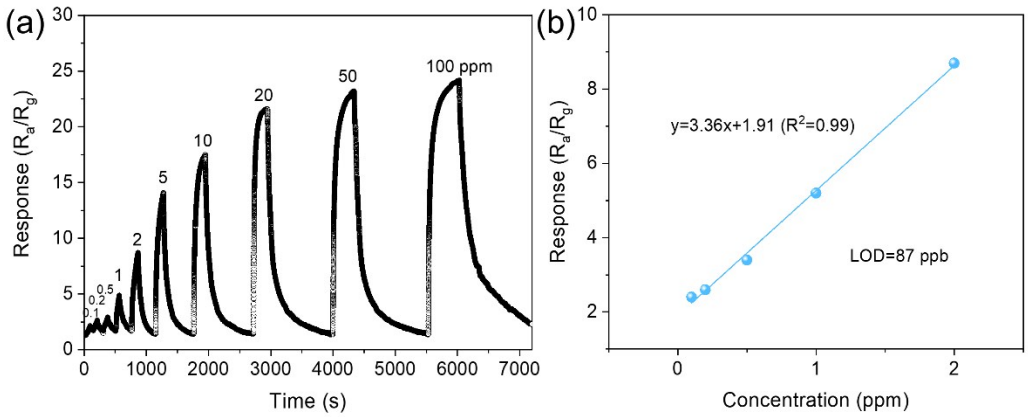

Figure S8. (a) Dynamic transients of SnO_2 thin films after annealing in Ar/H_2 to TEA concentration in the range of 0.1-100 ppm at 200 ^oC, and (b) linear fitting responses.

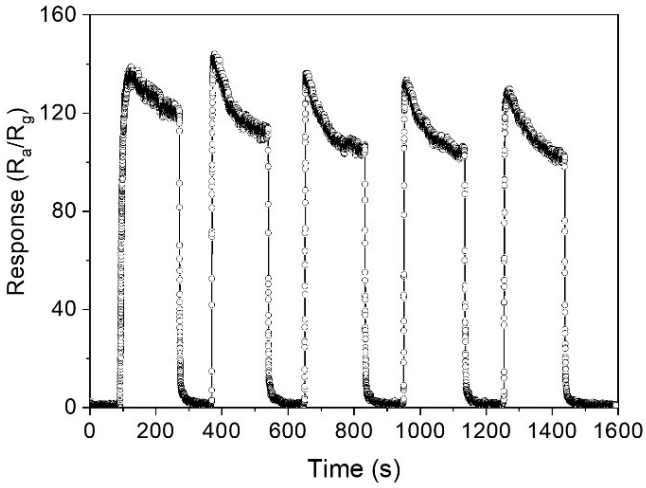

Figure S9. Dynamic transients on exposure to 10 ppm TEA of Pt/SnO_2 thin films for five consecutive tests.

Table S1. Comparison of TEA detection performances of various materials.

Materials	Operating temperature (°C)	Response/ppm	Response/recovery time (s)	LOD (ppm)
WO_3/SnO_2 nanoparticles[2]	220	87/50	6/7	1
NiO/SnO_2 hollow spheres[3]	220	46.5/10	11/34	2
SnO_2 hollow microfibers[4]	270	49.5/100	14/12	2
TiO_2/SnO_2 nanosheets[5]	260	52.3/100	12/22	2
Zn_2SnO_4/SnO_2 microspheres[6]	250	19.6/20	2/184	0.5
MoS_2/SnO_2 nanofibers[7]	230	106.3/200	-	5
Au/Mg-TiO_2/SnO_2 nanosheets[8]	260	30.43/50	9/95	2
Pd/In_2O_3 microstructures[9]	220	47.56/50	4/17	1
Al_2O_3/α-Fe_2O_3 nanofibers[10]	250	15.19/100	1/17	0.5
Au/ZnO nanorods[11]	40	22/50	11/15	1
Co_3O_4/In_2O_3 microtubes[12]	250	786.8/50	47/20	2
α-MoO_3 nanoflowers[13]	250	416/100	3/1283	0.5
Au/SnO_2/α-Fe_2O_3 nanoneedles[14]	300	39/100	4/203	2
$ZnCo_2O_4$ single-layer nanochain[15]	200	13/100	7/57	5
Au-TiO_2/m-CN	175	78.9/50	-	1

nanocomposite[16]				
Au/α-Fe_2O_3 nanorods[17]	40	17.5/50	12/8	1
In_2O_3 microtubes[18]	300	72/100	12/650	0.1
Au/Co_3O_4/$W_{18}O_{49}$ hollow spheres[19]	270	283.1/50	9/14	0.081
Pt/SnO_2 film (This work)	200	136.2/10	3/6	0.007

References

[1] V. V. Sysoev, B. K. Button, K. Wepsiec, S. Dmitriev, A. Kolmakov, *Nano Lett.*, 2006, **6**, 1584-1588.

[2] V. K. Tomer, S. Devi, R. Malik, S. P. Nehra, S. Duhan, *Sens. Actuators B*, 2016, **229**, 321-330.

[3] D. Ju, H. Xu, Q. Xu, H. Gong, Z. Qiu, J. Guo, J. Zhang, B. Cao, *Sens. Actuators B*, 2015, **215**, 39-44.

[4] Y. Zou, S. Chen, J. Sun, J. Liu, Y. Che, X. Liu, J. Zhang, D. Yang, *Acs Sens.*, 2017, **2**, 897-902.

[5] H. Xu, J. Ju, W. Li, J. Zhang, J. Wang, B. Cao, *Sens. Actuators B*, 2016, **228**, 634-642.

[6] X. Yang, Q. Yu, S. Zhang, P. Sun, H. Lu, X. Yan, F. Liu, X. Zhou, X. Liang, Y. Gao, G. Lu, *Sens. Actuators B*, 2018, **266**, 213-220.

[7] X. Q. Qao, Z. W. Zhang, D. F. Hou, D. S. Li, Y. L. Liu, Y. Q. Lan, J. Zhang, P. Y. Feng, X. H. Bu, *Acs Sustain. Chem. Eng.*, 2018, **6**, 12375-12384.

[8] H. Xu, D. Ju, Z. Chen, R. Han, T. Zhai, H. Yu, C. Liu, X. Wu, J. Wang, B. Cao, *Sens. Actuators B*, 2018, **273**, 328-335.

[9] X. Liu, K. Zhao, X. Sun, C. Zhang, X. Duan, P. Hou, G. Zhao, S. Zhang, H. Yang, R. Cao, X. Xu, *Sens. Actuators B*, 2019, **285**, 1-10.

[10] L. Guo, C. Wang, X. Kou, N. Xie, F. Liu, H. Zhang, X. Liang, Y. Gao, Y. Sun, X. Chuai, G. Lu, *Sens. Actuators B*, 2018, **266**, 139-148.

[11] X. Song, Q. Xu, H. Xu, B. Cao, *J. Colloid Interface Sci.*, 2017, **499**, 67-75.

[12] S. Shi, F. Zhang, H. Lin, Q. Wang, E. Shi, F. Qu, *Sens. Actuators B*, 2018, **262**, 739-749.

[13] L.-l. Sui, Y.-M. Xu, X.-F. Zhang, X.-L. Cheng, S. Gao, H. Zhao, Z. Cai, L.-H. Huo, *Sens. Actuators B*, 2015, **208**, 406-414.

[14] H. Xu, W. Li, R. Han, T. Zhai, H. Yu, Z. Chen, X. Wu, J. Wang, B. Cao, *Sens. Actuators B*, 2018, **262**, 70-78.

[15] N. Luo, G. Sun, B. Zhang, Y. Li, H. Jin, L. Lin, H. Bala, J. Cao, Z. Zhang, Y. Wang, *Sens. Actuators B*, 2018, **277**, 544-554.

[16] R. Malik, V. K. Tomer, N. Joshi, T. Dankwort, L. W. Lin, L. Kienle, *Acs Appl.*

Mater. Interfaces, 2018, **10**, 34087-34097.
[17] X. Song, Q. Xu, T. Zhang, B. Song, C. Li, B. Cao, *Sens. Actuators B*, 2018, **268**, 170-181.
[18] W. Yang, L. Feng, S. H. He, L. Y. Liu, S. T. Liu, *Acs Appl. Mater. Interfaces*, 2018, **10**, 27131-27140.
[19] Y. Xu, T. Ma, L. Zheng, L. Sun, X. Liu, Y. Zhao, J. Zhang, *Sens. Actuators B*, 2019, **284**, 202-212.